JOURNAL OF ENVIRONMENTAL SCIENCES 124 (2023) 678–687

Available online at www.sciencedirect.com

ScienceDirect

www.elsevier.com/locate/jes

JES JOURNAL OF ENVIRONMENTAL SCIENCES www.jesc.ac.cn

Variations in surface functional groups, carbon chemical state and graphitization degree during thermal deactivation of diesel soot particles

Ye Liu[1], *Sijin Wu*[1], *Chenyang Fan*[2,*], *Xin Wang*[2], *Fangjie Liu*[2], *Haibo Chen*[1]

[1] *Institute for Transport Studies, University of Leeds, Leeds LS2 9JT, UK*

[2] *Vehicle & Transportation Engineering Institute, Henan University of Science and Technology, Luoyang 471003, China*

ARTICLE INFO

Article history:
Received 5 August 2021
Revised 28 December 2021
Accepted 8 January 2022
Available online 15 January 2022

Keywords:
Diesel soot particles
Surface functional groups
Carbon chemical state
Graphitization degree
Thermal deactivation

ABSTRACT

The thermal deactivation of diesel soot particles exerts a significant influence on the control strategy for the regeneration of diesel particulate filters (DPFs). This work focused on the changes in the surface functional groups, carbon chemical state, and graphitization degree during thermal treatment in an inert gas environment at intermediate temperatures of 600°C, 800°C, and 1000°C and explore the chemical species that were desorbed from the diesel soot surface during thermal treatment using a thermogravimetric analyser coupled with a gas-chromatograph mass spectrometer (TGA-GC/MS). The surface functional groups and carbon chemical state were characterized using Fourier transform infrared spectroscopy (FT-IR) and X-ray photoelectron spectroscopy (XPS). The graphitization degree was evaluated by means of Raman spectroscopy (RS). The concentrations of aliphatic C–H, C–OH, C=O, and O–C=O groups are reduced for diesel soot and carbon black when increasing the thermal treatment temperature, while the sp^2/sp^3 hybridized ratio and graphitization degree enhance. These results provide comprehensive evidence of the decreased reactivity of soot samples. Among oxygenated functional groups, the percentage reduction during thermal treatment is the largest for the O–C=O groups owing to its worst thermodynamic stability. TGA-GC/MS results show that the aliphatic and aromatic chains and oxygenated species would be desorbed from the soot surface during 1000°C thermal treatment of diesel soot.

Introduction

Currently, diesel particulate filters (DPFs), as a common technology, are widely employed to reduce soot particle emissions and improve air quality (Schejbal et al., 2009; Suarez-Bertoa et al., 2019; Zardini et al., 2019). In DPFs, soot particles are trapped until these soot particles will be oxidized when DPF regeneration takes place. The high-temperature exhaust gases varying from 250 to 850°C during this process pass continuously through DPFs (Matsumoto et al., 2008; Raj et al., 2014; Roth et al., 1998). These trapped soot particles undergo thermal treatment for a long time in DPFs, which

* Corresponding author.
E-mails: fanchenyang@tju.edu.cn (C. Fan), h.chen@its.leeds.ac.uk (H. Chen).

https://doi.org/10.1016/j.jes.2022.01.007
1001-0742/

inevitably causes the thermal deactivation of diesel soot particles. Thermal deactivation means a reduction in reactivity upon thermal treatment (Sheng, 2007; Vander Wal et al., 2004), making diesel soot particles more resistant to be removed when the DPFs regenerate. Thus, it is necessary to probe the reason behind the thermal deactivation to further optimize the control strategy for the DPF regeneration.

Many studies have been conducted concerning the thermal deactivation of carbonaceous materials such as coal char, carbon black, and soot particles (Feng et al., 2002; Jaramillo et al., 2015; Raj et al., 2014; Sheng, 2007). For instance, Feng et al. (2002) studied the impact of thermal treatment in the range of 850°C–1150°C on the structure and reactivity of the coal char. The results indicated that the thermal deactivation was strongly dependent on the crystallite-perfecting process during thermal treatment. The same conclusions were reached by Sheng (2007), who reported that the increased structural ordering of char crystalline during thermal treatment between 1200°C and 1500°C was responsible for the thermal deactivation. Gaddam et al. (2016) studied the variation in the nanostructure and reactivity of the model carbons when heated to a temperature up to 3000°C under a He atmosphere. The crystallite growth and increase in density during thermal treatment were observed, which caused the decreased reactivity. Raj et al. (2014) performed a comprehensive study regarding thermal fragmentation and the change in soot reactivity during isothermal conditions in an inert environment at temperatures ranging from 400°C to 900°C. They had a deep understanding of the change of soot reactivity from the perspective of structural variation. Jaramillo et al. (2015) explored the changes in nanostructure and reactivity of three model carbons during oxidation at temperatures in the range of 575°C –775°C in air. The results presented a good relationship between oxidative reactivity and carbon nanostructure. Zolin et al. (2002) analysed the influence of thermal treatment in an oxygen environment on oxidative reactivity of coal char and found that the elimination of hydrogen and oxygen in the carbonaceous matrix and loss of edge active sites during thermal treatment would lead to a reduction in the oxidative reactivity. However, limited information regarding the changes in the surface functional groups, carbon chemical state, and graphitization degree of diesel soot particles during thermal deactivation is available in a nitrogen environment at temperatures ranging from 600°C to 1000°C. Although the exhaust gases passing through a DPF include several gas components, the nitrogen is approximately 70% or even more in these gases (Reşitoğlu et al., 2014). Moreover, the thermal treatment performed under only nitrogen conditions would eliminate the effect of other gas components on the experimental results.

Surface functional groups bonded to non-six-membered carbon during the soot oxidation process exert a crucial influence on soot structure and reactivity (Santamaria et al., 2006; Vander Wal et al., 2007; Yang et al., 2017). The thermal decomposition of these functional groups would chemically and physically weaken the barriers to lamella reorganization, favouring the rearrangement of carbon lamella and changing the nanostructure (Fernandes et al., 2003; Vander Wal et al., 2007). Simultaneously, the preferential loss of surface functional groups can enhance reactive sites, thereby increasing the soot reactivity (Agudelo et al., 2014; Soriano et al., 2017; Zhu et al., 2019). The sp^2 and sp^3 hybridized carbon atoms are primarily chemical states in soot, and the relative amount and spatial relationships are closely associated with the soot structure and reactivity (Vander Wal et al., 2016). In addition, the degree of graphitization is a vital indicator of soot structural order, which is strongly associated with the in-plane crystallite size, affecting soot reactivity (Liu et al., 2017; Sheng, 2007; Wei et al., 2015).

Table 1 – Detailed specifications of the diesel engine.

Engine parameters	
Number of cylinders, configuration	Four, in-line
Bore × stroke (mm)	102 × 108
Compression ratio	17:1
Engine displacement (L)	3.856
Rated power	100 kW@2800 r/min
Maximum torque (N·m)	420
Fuel injection type	Common rail system

In this context, the purpose of the present work is to study the alterations in surface functional groups, carbon chemical state and graphitization degree during thermal treatment of soot samples in an inert gas atmosphere at temperatures ranging from 600 to 1000°C and further explore the reason for thermal deactivation. The carbon chemical state and surface functional groups were characterized by means of X-ray photoelectron spectroscopy (XPS) and Fourier transform infrared spectroscopy (FT-IR). The graphitization degree of soot particles was evaluated using Raman spectroscopy (RS). Moreover, a thermogravimetric analyser coupled with a gas-chromatograph mass spectrometer (TGA-GC/MS) was used to explore the chemical species that were desorbed from the diesel soot surface during thermal treatment.

1. Experimental setup

1.1. *Soot samples*

Diesel soot particles were sampled on Teflon filters (R2PL047, PALL, USA) from a four-cylinder, four-stroke and turbocharged compression ignition diesel engine. Table 1 lists the details of the engine used. The engine operating load and speed were set at 55% of the full load and 1800 r/min. Fig. 1 shows the sample collection system, primarily including a filter supporter, a flowmeter, and a vacuum pump. The sample flow rate was set at 1 L/s, and the temperature of the sample

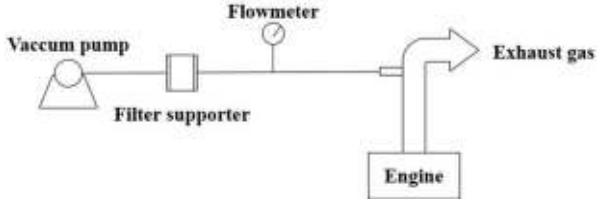

Fig. 1 – A schematic of the sample collection system (Liu et al., 2022).

zone was controlled at 55 ± 5 °C. Diesel soot particles were collected from the raw exhaust pipeline of the diesel engine onto the Teflon filters (R2PL047, PALL, USA) using a vacuum pump. After sampling, the soot samples were scripted from Teflon filters using a micro-spoon made of stainless steel. The soot samples were scraped from the filters after sampling for further thermal treatment. Additionally, the Printex-U, a commercial carbon black from Evonik-Degussa, was also examined to compare the properties of the diesel soot and Printex-U because the Printex-U is frequently employed as a surrogate for diesel soot (Raj et al., 2013; Vander Wal et al., 2007).

1.2. *Thermal treatment*

For each thermal treatment, 5 mg of the soot sample in platinum crucibles of TGA was performed under a nitrogen atmosphere. The nitrogen environment chosen for thermal treatment is because the nitrogen is approximately 70% or even more in the exhaust gases passing through a DPF (Reşitoğlu et al., 2014). Moreover, the thermal treatment performed under only a nitrogen environment would isolate the effect of other gas components of exhaust gases on experimental results. Previous studies have demonstrated that thermal treatment at 450°C for 60 min under an inert gas condition could effectively remove the absorbed unburned hydrocarbons and volatile matters and exert a limited influence on soot properties (Yehliu et al., 2013; Yehliu et al., 2012). Thus, the temperature was heated to 450°C at first and kept this temperature for 60 min, which causes the desorption of the volatiles such as loosely-bound hydrocarbons and water vapour (Raj et al., 2014; Yehliu et al., 2013). The devolatalised diesel soot and carbon black were termed DS-D and CB-D. Then the isothermally thermal treatment was carried out under various temperatures for seven hours. The significant thermal deactivation occurs when the thermal treatment temperature is above 500°C in an inert gas condition (Gaddam et al., 2016; Raj et al., 2014). Consequently, 600°C, 800°C, and 1000°C were chosen as isothermal thermal treatment temperatures to study the variations in soot properties during the thermal deactivation of soot particles. The diesel soot and carbon black after thermal treatment at 600°C, 800°C, and 1000°C are denoted as DS-600, DS-800, DS-1000, CB-600, CB-800, and CB-1000, respectively.

The mass loss of diesel soot and carbon black against the treatment time under various temperatures has been reported and discussed in detail in our previous work (Liu et al., 2022). It is found that the mass loss at 1000°C is observed to be up to 28.3% for diesel soot and 25.6% for carbon black. To explore the chemical species that were desorbed from the soot sample during thermal treatment, a thermogravimetric analyzer coupled with a gas-chromatograph mass spectrometer (TGA-GC/MS) was used in the present work. The previous study has confirmed that the results in terms of mass loss kinetics under an inert gas (nitrogen and helium) environment are the same (González Martínez et al., 2018). Therefore, Helium that is the common-used carrier gas in GC/MS analysis, was used as the carrier gas during 1000°C isothermal treatment of diesel soot in TGA. After 3 hours of isothermal treatment at 1000°C, the discharge gases from TGA were injected in GC/MS (Agilent 7890 A/5975C) through a heated line that is made of stainless steel and was maintained at 300°C. Through a multiport valving mechanism, the GC was equipped both with an HP-5 column, which was directly interfaced to the mass spectrometer, and with the packed column, which was connected to a thermal conductivity detector (TCD). Table 2 shows species detected from the discharge gases of TGA during thermal treatment of diesel soot at 1000°C. From this Table 2, major species, such as carbon monoxide, ethylene, ethane, methanol, 1-butyne, cyclopentadiene and toluene, were detected in the discharge gases of TGA. It means that desorption of the aliphatic and aromatic chains and oxygenated species from the soot surface would occur during the thermal treatment of diesel soot under an inert gas atmosphere. These species removed from soot surface during thermal treatment were determined based on: (1) their GC retention time; (2) their mass spectra with reference to the National Institute of Science and Technology (NIST) spectrum library; (3) published mass spectra in relevant studies (Castaldi et al., 1995; Song and Peng, 2010).

Table 2 – Species detected from the discharge gases during thermal treatment.

Species	Name	Quantification method	Molecular weight
CO	Carbon monoxide	TCD	28
C_2H_4	Ethylene	TCD	28
C_2H_6	Ethane	TCD	30
CH_3OH	Methanol	TCD	32
C_4H_6	1-Butyne	MS	54
C_5H_6	Cyclopentadiene	MS	66
C_7H_8	Toluene	MS	92

TCD: thermal conductivity detector; MS: mass spectrometer.

1.3. *FT-IR*

FT-IR was used to identify the surface functional groups on the soot surface. FT-IR spectrometer (Nicolet Nexus 470) was employed with a spectral range of 600–3200 cm^{-1} and a resolution of 1 cm^{-1}. The soot samples and analysis grade KBr in the proportion of 0.5 wt.% were mixed and ground, and mixed dispersions were compressed for 5 min at 10 Ton into a thin disk. Each sample was repeated four times to evaluate reproducibility. The uncertainty of the measurement of FT-IR spectra was less than 7%.

1.4. *XPS*

XPS was implemented to acquire information on the oxygenated functional group and the carbon chemical state in the soot samples. A PerkinElmer PHI-1600 ESCA spectrometer was employed to record XPS spectra using an Mg $K\alpha$ X-ray source operated at ultra-high vacuum conditions. The C1s peak of contaminant carbon (BE = 284.6 eV) was served as an internal standard to calibrate the binding energies. More than three spectra for each sample were obtained to make sure the reproducibility of the tested results.

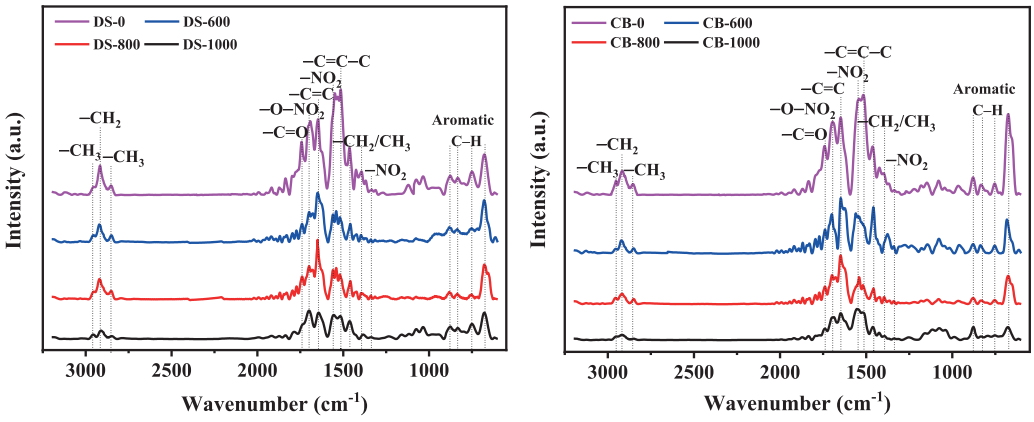

Fig. 2 – FT-IR spectra of diesel soot and carbon black over thermal treatment at various temperatures.

1.5. *Raman spectra*

Raman spectra were measured by means of Raman microscope system (Renishaw 1000) with a wavelength of 514.5 nm and an Ar ion excitation laser. Raman spectra in the 900–2000 cm^{-1} range were recorded with an exposure time of 60 s. About 1 mW laser beam power was employed to avoid modifying or burning the soot samples. For each sample, more than three spectra were obtained to make sure the reproducibility of the results.

2. Results and discussion

2.1. *Surface functional groups*

In the present study, FT-IR was used to identify surface functional groups on the soot surfaces. Fig. 2 shows the background-corrected, smoothed FT-IR spectra of diesel soot and carbon black over thermal treatment at various temperatures in the region between 600 and 3200 cm^{-1}. All the soot samples have almost similar positions of peaks but exhibit different signal intensities. Three well-defined aliphatic CH_3 asymmetric stretching, CH_2 asymmetric stretching and CH_3 symmetric stretching peaks are measured at 2960, 2920, and 2850 cm^{-1}, respectively, which are primarily from methylene bridges maintaining the interconnection among PAHs or from methyl, methylene, and methine attached to aromatic rings on PAHs (Ibarra et al., 1996; Liu et al., 2016; Santamaria et al., 2006). The aliphatic C–H plane deformations of CH_2/CH_3 groups are measured and located at 1380 and 1450 cm^{-1}, respectively (Cain et al., 2010; Santamaria et al., 2006). Most of the peaks detected here are also observed for soot particles formed in an inverse diffusion flame (Santamaria et al., 2006; Santamaria et al., 2010). However, no signal of aromatic C–H stretching located at around 3030 cm^{-1} is measured in this study. The aromatic out-of-plane C–H bending vibrations of three-adjacent, two-adjacent and isolated hydrogens are observed at 750, 830, and 880 cm^{-1}, respectively (Russo et al., 2014; Santamaria et al., 2006). The peak at 675 cm^{-1} is measured in this study, which is assigned to aromatic out-of-plane C–H bending vibration (Bladt et al., 2012). The peaks at 1640 and 1520 cm^{-1} are detected, corresponding to the stretching of alkenyl C=C and aromatic C=C–C groups (Raj et al., 2014; Santamaria et al., 2006). Some oxygen-related functional groups are also measured for the soot samples. The peak of C=O stretching of carboxylic groups is observed at about 1720 cm^{-1} (Kirchner et al., 2000; McKinnon et al., 1996). The oxygen-carbon stretching groups of the ether, esters and hydroxyl appear at 1260, 1100, and 1050 cm^{-1}, respectively (Cain et al., 2010). In addition, the nitro compounds ($-NO_2$) are detected at around 1560 cm^{-1} and 1320 cm^{-1} (Popovicheva et al., 2015; Tapia et al., 2018), and the organic nitrate ($-O-NO_2$) is observed at about 1670 cm^{-1} (Chughtai et al., 1994; Kirchner et al., 2000).

2.1.1. Aliphatic and aromatic C–H groups

Given some factors, such as the content and thickness of the KBr pellet, have an impact on the signal intensity in FT-IR spectra, the intensity ratio of the aliphatic C–H peak at 2920 cm^{-1} to the aromatic C=C peak at 1640 cm^{-1} ($I_{Ali}/I_{C=C}$) is used to quantify the relative concentration of aliphatic C–H groups in the light of the suggestion by McKinnon et al. (1996) and Santamaría et al. (2007). Fig. 3 presents the variation in the $I_{Ali}/I_{C=C}$ ratios as functions of thermal treatment temperatures. The diesel soot and carbon black exhibit the same evolution trend regarding changes in the $I_{Ali}/I_{C=C}$ ratios when increasing thermal treatment temperature. The relative content of aliphatic C–H groups reduces gradually with an increase in thermal treatment temperature, indicating that the higher thermal treatment temperature would consume more aliphatic hydrogen. This behaviour is primarily ascribed to the following factors: (1) the increased carbonization reactions with increasing thermal treatment temperatures enhance dehydrogenation rates (Liu et al., 2016; Wang et al., 2013); (2) the decomposition of the aliphatics, such as aliphatic C–H groups on soot surfaces, would occur when heated at higher thermal treatment temperature (Raj et al., 2014). In the study of the soot carbonization process by Vander Wal (1998), it was found that carbonization reduced the concentration of hydrogen functional groups. (Dobbins et al., 1995; Dobbins et al., 1996) stated that the carbonization reaction would reduce aliphatic C–H functional groups on soot surfaces.

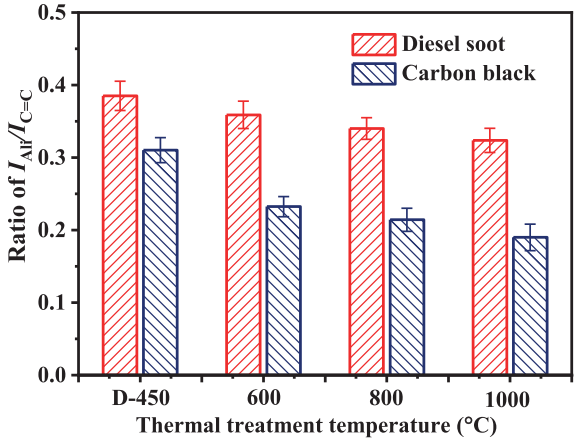

Fig. 3 – Relative concentrations of aliphatic C–H functional groups as functions of thermal treatment temperature. The error bars indicate the standard error.

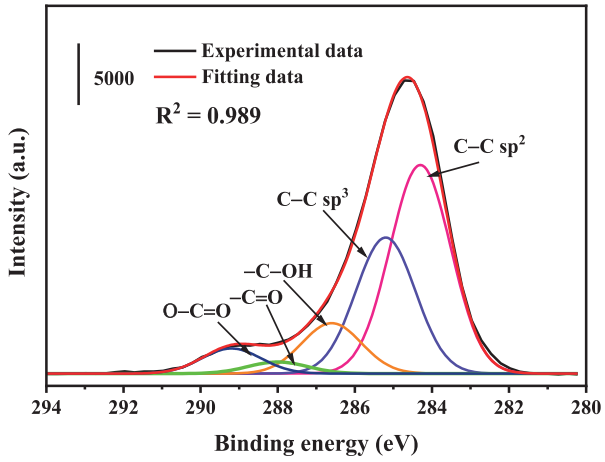

Fig. 4 – Representative XPS C 1s narrow spectra for DS-D.

Aliphatic C–H groups are a crucial factor affecting soot oxidation reactivity (Wang et al., 2013). The abstraction of H-atoms in aliphatic C–H groups requires lower energy, and the preferential loss of aliphatic hydrogen enhances the number of active sites, increasing soot reactivity (Santamaria et al., 2006). As a result, the concentration of aliphatic C–H functional groups reduces when increasing thermal treatment temperature, which decreases the number of actives sites and lowers soot reactivity. Agudelo et al. (2014) investigated the soot particles from diesel and crude vegetable oils. The results presented that the reduction in aliphatic C–H groups led to the decreased reactivity. The same conclusion was reached by Ruiz et al. (2015), who found that the soot reactivity reduced as the concentration of aliphatic C–H groups decreased. Soriano et al. (2017) discovered that soot generated from paraffinic fuel had higher reactivity than that from diesel fuel. They revealed that this higher reactivity was due to a higher concentration of aliphatic functional groups.

2.1.2. *Oxygenated functional groups*

XPS analyses in this study were carried out to gain information regarding the oxygenated functional groups and carbon chemical state. **Fig. 4** presents a representative high-resolution scan of the C1s peak. The C1s region was deconvoluted to four peaks according to the method suggested in the literature (Gaddam and Vander Wal, 2013; Pumera and Iwai, 2009): the peak at 286.6 eV assigned to hydroxyl (C–OH) groups, the peak at 288.4 eV corresponding to carbonyl (C=O) group, and the peak at 289.2 eV referring to the carboxylic acid (O–C=O) group. The analysis of sp^2 and sp^3 hybridized carbons will be discussed in detail in the subsequent section. The concentrations of C–OH, O–C=O and C=O groups for diesel soot and carbon black are plotted against thermal treatment temperatures in **Fig. 5**. The contents of C–OH, O–C=O and C=O groups reduce when increasing the thermal treatment temperature, indicating that the more oxygenated functional groups are desorbed at the higher temperature. According to previous work (Lapuerta et al., 2020; Song et al., 2007), the oxygenated groups are important intermediate compounds and exert a crucial influence on oxidation reaction, influencing soot reactivity. In the present work, the oxygenated functional groups for soot samples decrease with the increase in thermal treatment temperature, which in turn reduced soot reactivity. Song et al. (2006) probed the correlation between the oxygenated functional groups and reactivity and found that the decreased relative concentration of oxygenated functional groups would reduce soot reactivity. Soriano et al. (2017) came to the same conclusion, and the results revealed that the biodiesel soot possessed higher concentrations of oxygenated functional groups compared to diesel soot and had higher oxidative reactivity. However, a different conclusion was obtained by Yehliu et al. (2012), who found that the content of oxygenated functional groups was not associated with soot reactivity.

The percentage reductions of C–OH, C=O and O–C=O groups for diesel soot and carbon black are calculated with various thermal treatment temperatures. Compared to DS-D, the concentrations of C–OH, C=O and O–C=O groups for DS-1000 reduce by 31%, 37%, and 44%. Similarly, the contents of C–OH, C=O and O–C=O groups for CB-1000 decrease by 34%, 38% and 47% than those for CB-D. The percentage reduction for diesel soot and carbon black follows the sequence: O–C=O > C=O > C–OH groups, which is likely to be correlated with the relative thermodynamic stability of these oxygenated functional groups. In the study by Vander Wal et al. (2010), it was discovered that the relative thermodynamic stability of C–OH, C=O and O–C=O groups decreases sequentially. As a result, the O–C=O groups have the worst thermodynamic stability, and thus the percentage reduction is the largest for the O–C=O groups.

2.2. *Carbon chemical state*

XPS was also used to gain chemical information regarding the sp^2 and sp^3 hybridized carbon atoms (Tandon and Rosner, 1996; Vander Wal et al., 2014). The sp^2 and sp^3 hybridized carbon atoms are integral to the overall soot nanostructure. As shown in **Fig. 4**, the deconvolution of the high-resolution spectrum about the C1s region was performed to quantify the relative contents of sp^2 and sp^3 hybridized carbon atoms.

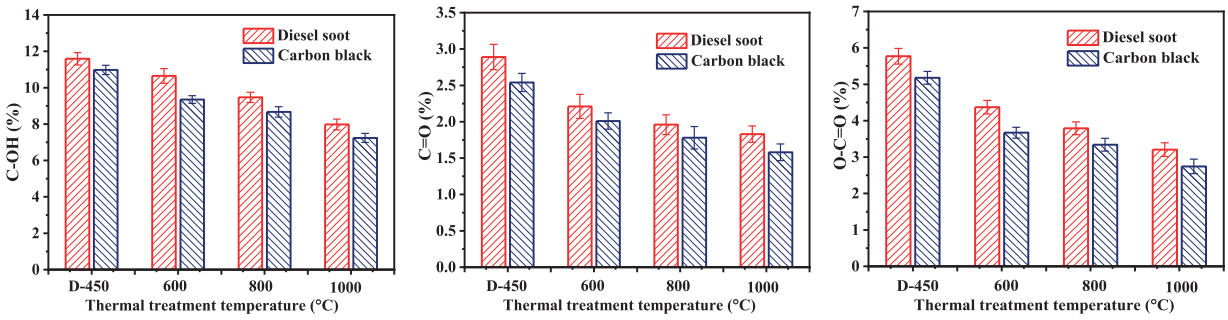

Fig. 5 – Contents of C–OH, O–C=O and C=O groups as functions of thermal treatment temperature. The error bars indicate the standard error.

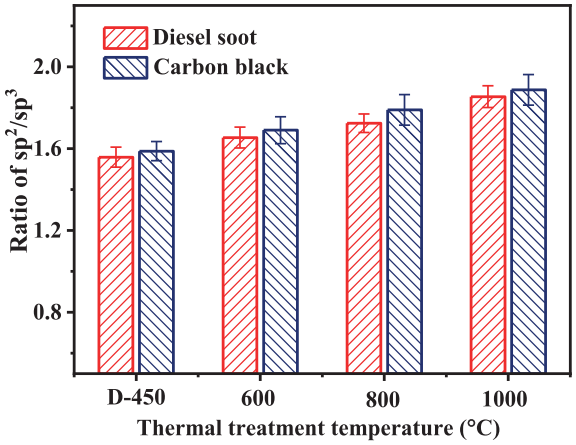

Fig. 6 – Sp^2/sp^3 hybridization ratios as functions of thermal treatment temperature. The error bars indicate the standard error.

The peak near 284.3 eV is a representation of sp^2 hybridized carbons and π bonding in soot (Guerrero Peña et al., 2016; Raj et al., 2014). The peak near 285.2 eV is assigned to the sp^3 hybridized carbons and σ bonding in soot (Guerrero Peña et al., 2016; Raj et al., 2014). The sp^2 hybridized carbons refer to the ordered carbon, and the sp^3 hybridized carbon atoms would affect the sp^2 hybridized network and need bond terminations other than adjacent π bonded carbon atoms. These sp^3 hybridized carbon atoms would reduce the structural order and are consequently considered as the defect sites (Vander Wal et al., 2011). Thus, a large sp^2/sp^3 hybridization ratio corresponds to a more ordered structure (Alfè et al., 2009).

Fig. 6 shows the sp^2/sp^3 values for diesel soot and carbon black as functions of thermal treatment temperature. Compared to diesel soot, carbon black has slightly larger sp^2/sp^3 values at each thermal treatment temperature. In addition, a monotonic increase trend in sp^2/sp^3 hybridization ratios for diesel soot and carbon black is observed with increasing thermal treatment temperature, demonstrating that soot samples transform towards a more ordered structure as thermal treatment temperature increases. This behavior is primarily due to the decomposition of more amorphous species on soot surfaces when increasing thermal treatment temperature. Raj et al. (2014) also reported that amorphous and disorder species were desorbed from soot surfaces, which included a large quantity of cyclic or acyclic aliphatics. In the study by Fetzer (2000), it was found that some amorphous PAHs making up soot particles would be sublimated at approximately 500°C. Consequently, more amorphous PAHs will be sublimated when heated above 500°C, which favours soot samples towards a better graphitic organization, corresponding to the increased sp^2/sp^3 ratio. In addition, it was found through a theoretical calculation that the binding energy of the PAHs on soot surfaces was closely related to the mass of PAHs in the stack, and small PAHs had lower binding energy relative to the large ones (Herdman and Miller, 2008; Raj et al., 2011). As a result, there is a high probability for amorphous and small PAHs that can escape from the PAHs stacks in soot by overcoming van der Waals force of attraction, which develops a more ordered structure, in line with the current XPS data. An increase in sp^2/sp^3 hybridization ratio corresponds to an enhancement in graphitic planar structures within soot samples, which reduces active sites for oxygen attack and thus lowers soot reactivity (Alfè et al., 2009). A similar finding was reported by Gaddam et al. (2016), who pointed out that the large sp^2/sp^3 hybridization ratio for the model carbon presented low reactivity. Fan et al. (2019) revealed that the diesel soot particles with the large sp^2/sp^3 hybridization ratio presented more resistance to oxidation.

2.3. *Graphitization degree*

RS was employed to assess the graphitization degree of the soot samples. Fig. 7 shows the representative baseline-corrected, smoothed spectra of DS-1000 and CB-1000. It can be observed that these two spectra show two broad peaks at around 1350 cm^{-1} (D peak) and 1600 cm^{-1} (G peak). For quantitative analysis, the spectrum of each soot sample is deconvoluted and fitted by three Lorentian functions and one Gaussian function (Seong and Boehman, 2013), as shown in Fig. 8. The Lorentzian functions refer to the D1 band assigned to the carbon atoms at the edge sites of the graphene layers (Seong and Boehman, 2011), the D4 band arising from the C=C and C–C bands (Cuesta et al., 1994; Dippel et al., 1999), and the G band as a result of the ideal graphitic lattice (Seong and Boehman, 2013), while the Gaussian function corresponds to

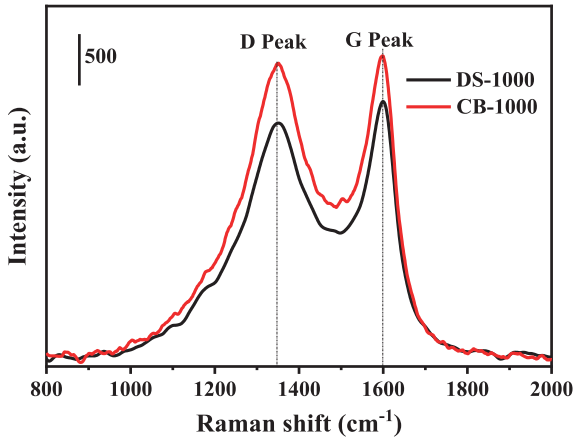

Fig. 7 – Representative Raman spectra of DS-1000 and CB-1000.

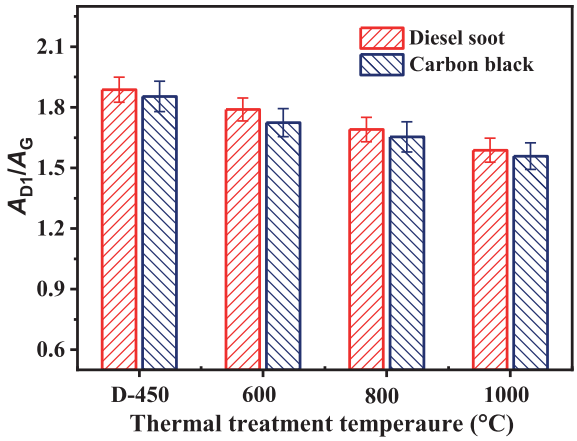

Fig. 9 – A_{D1}/A_G ratios as functions of thermal treatment temperature. The error bars indicate the standard error.

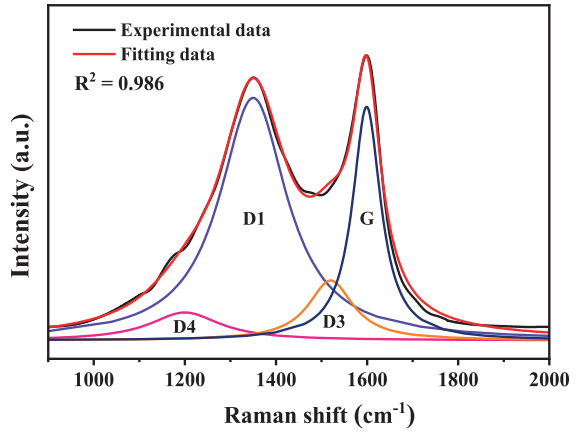

Fig. 8 – Four-band fitting of representative Raman spectrum for DS-1000.

the D3 band arising from the amorphous carbon of the soot (Cuesta et al., 1994; Parent et al., 2016).

The peak intensity ratios of the D1 band or the full width at half maximum (FWHM) of the bands to the G band were frequently employed to determine the graphitization degree of carbon materials (Sheng, 2007; Yoshida et al., 2006; Zaida et al., 2007). However, only the peak intensity ratio or the FWHM of the bands is likely unable to be a complete representation of the evolution of soot structural order. By contrast, the peak area ratio (integrated intensity) is the function of the FWHM and the peak intensity, which includes the effect of these two parameters. As a result, the peak area ratios of D1 to G (A_{D1}/A_G) are used to evaluate the graphitization degree of soot samples in the present study. A lower A_{D1}/A_G ratio indicates a more ordered structure in soot (Sheng, 2007; Tuinstra and Koenig, 1970). Fig. 9 shows the change in graphitization degree of soot samples against various thermal treatment temperatures. Compared to diesel soot, the carbon black is observed to have a lower value of A_{D1}/A_G ratio at the same thermal treatment temperature. For the diesel soot and carbon black, the values of A_{D1}/A_G reduce from 1.89 to 1.59 and from 1.85 to 1.56 with the temperature increasing from 600 to 1000°C, respectively, indicating the transformation towards more-ordered structure for both soot samples. Such a structural transformation is mainly because the amorphous species on the soot surfaces are desorbed during thermal treatment (Raj et al., 2014; Sheng, 2007; Zaida et al., 2007). Compared to carbon atoms in the basal plane, the carbon atoms at the edge sites of the graphene were reported to have 100-1000 times more reactive (Marsh and Kuo, 1989; Vander Wal and Mueller, 2006; Vander Wal and Tomasek, 2004). The thermally treated soot samples possess more ordering of the soot crystallite structure, corresponding to the lower ratio of edge to base carbon atoms. As a result, soot samples after thermal treatment present more resistance towards oxidation. A similar finding was reported by Sheng (2007), who studied the structure and reactivity of coal chars under different thermal treatment conditions and identified that the thermal deactivation of coal char was dependent on the structural ordering of char crystallite. Feng et al. (2002) probed the change in the structural ordering of coal char during thermal treatment and the effect on its reactivity. The results revealed that the decrease in reactivity during thermal treatment was due to a crystallite-perfecting process. Raj et al. (2014) believed that thermal treatment decreased the number of carbon atoms at the edge sites for reaction, thus lowering soot reactivity.

Close observation of Figs. 3, 5, 6, and 9 present that considering the uncertainties of aliphatic C–H groups, oxygenated functional groups, sp^2/sp^3 ratio, and A_{D1}/A_G ratio, it appears to be no significant difference in the average values among these properties of thermally treated samples. To determine the statistical differences, the statistical analysis, one-way analysis of variance (ANOVA), was conducted. For all results, the p values obtained from the statistical analysis are lower than 0.05, suggesting that such differences are statistically significant. It is worth mentioning that the Printex-U in the previous studies was frequently employed as a surrogate for diesel soot (Arnal et al., 2012; Vander Wal et al., 2007). However, our current results show that the aliphatic C–H groups, oxygenated functional groups, carbon chemical state and graphitization degree for diesel soot are statistically different from those for the Printex-U, which is likely due to a lower proportion in

heteroatoms and a higher graphitic order for the Printex-U (Jaramillo et al., 2015). In a study by Tapia et al. (2015), they also reported that there were significant differences in surface functional group density between Printex and diesel soot samples. Additionally, soot properties emitted from a diesel engine are affected significantly by diesel engine type, engine speed and engine load (Lapuerta et al., 2020). As a result, whether the Printex-U can be employed as the best surrogate for diesel soot to perform related research remains to be further studied. Furthermore, it is worth mentioning that in addition to nitrogen, there are oxygen, carbon dioxide, and nitric oxide in the diesel exhaust. To distinguish the thermal effect from the oxidation reaction effect, only nitrogen was chosen for thermal treatment in the current work to explore its effect on soot feature. In our further research, the separate effects of different gases in the diesel exhaust, such as oxygen, carbon dioxide, and nitric oxide, on soot features will be performed to identify the corresponding contribution for the change in soot properties.

The trapped soot particles in DPFs undergo thermal treatment because the high-temperature exhaust gases pass continuously through DPFs. Our current results show that the concentrations of aliphatic C–H groups, C–OH, C=O, and O–C=O groups for soot samples reduce after thermal treatment or with the increase in thermal treatment temperature, and the sp^2/sp^3 hybridized ratio and graphitization degree enhance, which lead to the reduction in soot reactivity. Thus, to avoid the occurrence of significantly thermal deactivation of diesel soot particles in DPFs that makes them more resistant to be removed when the DPFs regenerate, limiting extremely high engine load and speed seems to effective solution because the extremely high engine load and speed would correspond to high exhaust temperature. In addition, an increase in the frequency of DPF regeneration with a shorter regeneration time is recommended. For instance, the trapped soot particles would experience a short thermal treatment due to the increased frequency of DFP regeneration and thus have high reactivity. The trapped soot particles with high reactivity are more readily oxidised, and hence less fuel is required for the removal of these particles during DFP regeneration, which is beneficial to the environment.

3. Conclusions

Variations in surface functional groups, carbon chemical state and graphitization degree of diesel soot and a commercial carbon black were studied during thermal deactivation. The concentrations of aliphatic C–H groups, C–OH, C=O, and O–C=O groups reduce for diesel soot and carbon black when increasing thermal treatment temperature, whereas the sp^2/sp^3 hybridized ratio and graphitization degree enhance. These results can provide further evidence for thermal deactivation during thermal treatment. Compared to diesel soot, the commercial carbon black has lower concentrations of aliphatic C–H groups, C–OH, C=O and O–C=O groups and higher graphitization degree and sp^2/sp^3 hybridized ratio at the same thermal treatment temperature. Among oxygenated functional groups, the percentage reduction during thermal treatment is largest for the O–C=O groups due to its worst thermodynamic stability. TGA-GC/MS results show that the aliphatic and aromatic chains and oxygenated species would be desorbed from the soot surface during 1000°C thermal treatment of diesel soot under an inert gas atmosphere.

Acknowledgments

This work was supported by the National Natural Science Foundation of China (No. 52006054), the State Key Laboratory of Engines at Tianjin University (Grant No. K2021-05), and the European Union's projects MODALES (No. 815189) and nPETS (No. 954377).

REFERENCES

Agudelo, J.R., Álvarez, A., Armas, O., 2014. Impact of crude vegetable oils on the oxidation reactivity and nanostructure of diesel particulate matter. Combust. Flame 161 (11), 2904–2915.

Alfè, M., Apicella, B., Barbella, R., Rouzaud, J.N., Tregrossi, A., Ciajolo, A., 2009. Structure–property relationship in nanostructures of young and mature soot in premixed flames. Proc. Combust. Inst. 32 (1), 697–704.

Arnal, C., Alzueta, M.U., Millera, A., Bilbao, R., 2012. Influence of water vapor addition on soot oxidation at high temperature. Energy 43 (1), 55–63.

Bladt, H., Schmid, J., Kireeva, E.D., Popovicheva, O.B., Perseantseva, N.M., Timofeev, M.A., et al., 2012. Impact of Fe content in laboratory-produced soot aerosol on its composition, structure, and thermo-chemical properties. Aerosol Sci. Technol. 46 (12), 1337–1348.

Cain, J.P., Gassman, P.L., Wang, H., Laskin, A., 2010. Micro-FTIR study of soot chemical composition—evidence of aliphatic hydrocarbons on nascent soot surfaces. Phys. Chem. Chem. Phys. 12 (20), 5206.

Castaldi, M.J., Vincitore, A.M., Senkan, S.M., 1995. Micro-structures of premixed hydrocarbon flames: methane. Combust. Sci. Technol. 107 (1–3), 1–19.

Chughtai, A., Gordon, S., Smith, D., 1994. Kinetics of the hexane soot reaction with NO2/N2O4 at low concentration. Carbon 32 (3), 405–416.

Cuesta, A., Dhamelincourt, P., Laureyns, J., Martínez-Alonso, A., Tascón, J.M.D., 1994. Raman microprobe studies on carbon materials. Carbon 32 (8), 1523–1532.

Dippel, B., Janderb, H., Heintzenberga, J., 1999. NIR FT Raman spectroscopic study of flame soot. Phys. Chem. Chem. Phys. 1 (20), 4707–4712.

Dobbins, R.A., Fletcher, R.A., Lu, W., 1995. Laser microprobe analysis of soot precursor particles and carbonaceous soot. Combust. Flame 100 (1), 301–309.

Dobbins, R.A., Govatzidakis, G.J., Lu, W., Schwartzman, A.F., Fletcher, R.A., 1996. Carbonization Rate of Soot Precursor Particles. Combust. Sci. Technol. 121 (1–6), 103–121.

Fan, C., Song, C., Lv, G., Wei, J., Zhang, X., Qiao, Y., et al., 2019. Impact of post-injection strategy on the physicochemical properties and reactivity of diesel in-cylinder soot. Proc. Combust. Inst. 37 (4), 4821–4829.

Feng, B., Bhatia, S.K., Barry, J.C., 2002. Structural ordering of coal char during heat treatment and its impact on reactivity. Carbon 40 (4), 481–496.

Fernandes, M.B., Skjemstad, J.O., Johnson, B.B., Wells, J.D., Brooks, P., 2003. Characterization of carbonaceous combustion residues. I. Morphological, elemental and spectroscopic features. Chemosphere 51 (8), 785–795.

Fetzer, J.C., 2000. Large (C= 24) Polycyclic Aromatic Hydrocarbons: Chemistry And Analysis. John Wiley & Sons.
Gaddam, C.K., Vander Wal, R.L., 2013. Physical and chemical characterization of SIDI engine particulates. Combust. Flame 160 (11), 2517–2528.
Gaddam, C.K., Vander Wal, R.L., Chen, X., Yezerets, A., Kamasamudram, K., 2016. Reconciliation of carbon oxidation rates and activation energies based on changing nanostructure. Carbon 98, 545–556.
González Martínez, M., Dupont, C., Thiéry, S., Meyer, X.M., Gourdon, C., 2018. Impact of biomass diversity on torrefaction: study of solid conversion and volatile species formation through an innovative TGA-GC/MS apparatus. Biomass Bioenergy 119, 43–53.
Guerrero Peña, G.D.J., Alrefaai, M.M., Yang, S.Y., Raj, A., Brito, J.L., Stephen, S., et al., 2016. Effects of methyl group on aromatic hydrocarbons on the nanostructures and oxidative reactivity of combustion-generated soot. Combust. Flame 172, 1–12.
Herdman, J.D., Miller, J.H., 2008. Intermolecular potential calculations for polynuclear aromatic hydrocarbon clusters. J. Phys. Chem. A 112 (28), 6249–6256.
Ibarra, J., Muñoz, E., Moliner, R., 1996. FTIR study of the evolution of coal structure during the coalification process. Org. Geochem. 24, 725–735.
Jaramillo, I.C., Gaddam, C.K., Vander Wal, R.L., Lighty, J.S., 2015. Effect of nanostructure, oxidative pressure and extent of oxidation on model carbon reactivity. Combust. Flame 162 (5), 1848–1856.
Kirchner, U., Scheer, V., Vogt, R., 2000. FTIR Spectroscopic Investigation of the Mechanism and Kinetics of the Heterogeneous Reactions of NO2 and HNO3 with Soot. J. Phys. Chem. A 104 (39), 8908–8915.
Lapuerta, M., Rodríguez–Fernández, J., Sánchez-Valdepeñas, J., 2020. Soot reactivity analysis and implications on diesel filter regeneration. Prog. Energy Combust. Sci. 78, 100833.
Liu, Y., Fan, C., Wang, X., Liu, F., Chen, H., 2022. Thermally induced variations in the nanostructure and reactivity of soot particles emitted from a diesel engine. Chemosphere 286, 131712.
Liu, Y., Song, C., Lv, G., Cao, X., Wang, L., Qiao, Y., et al., 2016. Surface functional groups and sp 3/sp2 hybridization ratios of in-cylinder soot from a diesel engine fueled with n-heptane and n-heptane/toluene. Fuel 179, 108–113.
Liu, Y., Song, C., Lv, G., Wang, X., Li, N., 2017. Virgin and Extracted Soots in Premixed Methane Flames: A comparison of surface functional groups, graphitization degree, and oxidation reactivity. Energy Fuels 31 (6), 6413–6421.
Marsh, H., Kuo, K., 1989. Kinetics and catalysis of carbon gasification, Introduction to carbon science. Elsevier, pp. 107–151.
Matsumoto, K., Tojo, M., Jinnai, Y., Hayashi, N., Ibaraki, S., 2008. Development of compact and high-performance turbocharger for 1,050 C exhaust gas. Mitsubishi Heavy Ind. Tech. Rev. 45 (3), 1–5.
McKinnon, J.T., Meyer, E., Howard, J.B., 1996. Infrared analysis of flame-generated PAH samples. Combust. Flame 105 (1), 161–166.
Parent, P., Laffon, C., Marhaba, I., Ferry, D., Regier, T.Z., Ortega, I.K., et al., 2016. Nanoscale characterization of aircraft soot: A high-resolution transmission electron microscopy, Raman spectroscopy, X-ray photoelectron and near-edge X-ray absorption spectroscopy study. Carbon 101, 86–100.
Popovicheva, O.B., Kireeva, E.D., Shonija, N.K., Vojtisek-Lom, M., Schwarz, J., 2015. FTIR analysis of surface functionalities on particulate matter produced by off-road diesel engines operating on diesel and biofuel. Environ. Sci. Pollut. Res. 22 (6), 4534–4544.
Pumera, M., Iwai, H., 2009. Multicomponent metallic impurities and their influence upon the electrochemistry of carbon nanotubes. J. Phys. Chem. C 113 (11), 4401–4405.
Raj, A., Tayouo, R., Cha, D., Li, L., Ismail, M.A., Chung, S.H., 2014. Thermal fragmentation and deactivation of combustion-generated soot particles. Combust. Flame 161 (9), 2446–2457.
Raj, A., Yang, S.Y., Cha, D., Tayouo, R., Chung, S.H., 2013. Structural effects on the oxidation of soot particles by O2: experimental and theoretical study. Combust. Flame 160 (9), 1812–1826.
Raj, A., Zainuddin, Z., Sander, M., Kraft, M., 2011. A mechanistic study on the simultaneous elimination of soot and nitric oxide from engine exhaust. Carbon 49 (5), 1516–1531.
Reşitoğlu, I.A., Altinişik, K., Keskin, A., 2014. The pollutant emissions from diesel-engine vehicles and exhaust aftertreatment systems. Clean Technol. Environ. Policy 17 (1), 15–27.
Roth, P., Eckhardt, T., Franz, B., Patschull, J., 1998. H2O2-assisted regeneration of diesel particulate traps at typical exhaust gas temperatures. Combust. Flame 115 (1–2), 28–37.
Ruiz, F.A., Cadrazco, M., López, A.F., Sanchez-Valdepeñas, J., Agudelo, J.R., 2015. Impact of dual-fuel combustion with n-butanol or hydrous ethanol on the oxidation reactivity and nanostructure of diesel particulate matter. Fuel 161, 18–25.
Russo, C., Stanzione, F., Tregrossi, A., Ciajolo, A., 2014. Infrared spectroscopy of some carbon-based materials relevant in combustion: qualitative and quantitative analysis of hydrogen. Carbon 74, 127–138.
Santamaria, A., Mondragon, F., Molina, A., Marsh, N., Eddings, E., Sarofim, A., 2006. FT-IR and 1H NMR characterization of the products of an ethylene inverse diffusion flame. Combust. Flame 146 (1–2), 52–62.
Santamaría, A., Mondragón, F., Quiñónez, W., Eddings, E.G., Sarofim, A.F., 2007. Average structural analysis of the extractable material of young soot gathered in an ethylene inverse diffusion flame. Fuel 86 (12–13), 1908–1917.
Santamaria, A., Yang, N., Eddings, E., Mondragon, F., 2010. Chemical and morphological characterization of soot and soot precursors generated in an inverse diffusion flame with aromatic and aliphatic fuels. Combust. Flame 157 (1), 33–42.
Schejbal, M., Marek, M., Kubíček, M., Kočí, P., 2009. Modelling of diesel filters for particulates removal. Chem. Eng. J. 154 (1–3), 219–230.
Seong, H.J., Boehman, A.L., 2011. Impact of intake oxygen enrichment on oxidative reactivity and properties of diesel soot. Energy Fuels 25 (2), 602–616.
Seong, H.J., Boehman, A.L., 2013. Evaluation of raman parameters using visible raman microscopy for soot oxidative reactivity. Energy Fuels 27 (3), 1613–1624.
Sheng, C., 2007. Char structure characterised by Raman spectroscopy and its correlations with combustion reactivity. Fuel 86 (15), 2316–2324.
Song, J., Alam, M., Boehman, A.L., 2007. Impact of alternative fuels on soot properties and DPF regeneration. Combust. Sci. Technol. 179 (9), 1991–2037.
Song, J., Alam, M., Boehman, A.L., Kim, U., 2006. Examination of the oxidation behavior of biodiesel soot. Combust. Flame 146 (4), 589–604.
Song, J., Peng, P.a., 2010. Characterisation of black carbon materials by pyrolysis–gas chromatography–mass spectrometry. J. Anal. Appl. Pyrolysis 87 (1), 129–137.
Soriano, J.A., Agudelo, J.R., López, A.F., Armas, O., 2017. Oxidation reactivity and nanostructural characterization of the soot coming from farnesane-A novel diesel fuel derived from sugar cane. Carbon 125, 516–529.
Suarez-Bertoa, R., Valverde, V., Clairotte, M., Pavlovic, J., Giechaskiel, B., Franco, V., et al., 2019. On-road emissions of passenger cars beyond the boundary conditions of the real-driving emissions test. Environ. Res. 176, 108572.

Tandon, P., Rosner, D.E., 1996. Sintering kinetics and transport property evolution of large multi-particle aggregates. Chem. Eng. Commun. 151 (1), 147–168.
Tapia, A., Salgado, M.S., Martín, M.P., Sánchez-Valdepeñas, J., Rossi, M.J., Cabañas, B., 2015. The use of heterogeneous chemistry for the characterization of functional groups at the gas/particle interface of soot from a diesel engine at a particular running condition. Environ. Sci. Pollut. Res. 22 (7), 4863–4872.
Tapia, A., Salgado, S., Martín, P., Villanueva, F., García-Contreras, R., Cabañas, B., 2018. Chemical composition and heterogeneous reactivity of soot generated in the combustion of diesel and GTL (Gas-to-Liquid) fuels and amorphous carbon Printex U with NO2 and CF3COOH gases. Atmos. Environ. 177, 214–221.
Tuinstra, F., Koenig, J.L., 1970. Raman spectrum of graphite. J. Chem. Phys. 53 (3), 1126–1130.
Vander Wal, R.L., 1998. Soot precursor carbonization: Visualization using LIF and LII and comparison using bright and dark field TEM. Combust. Flame 112 (4), 607–616.
Vander Wal, R.L., Bryg, V.M., Hays, M.D., 2010. Fingerprinting soot (towards source identification): Physical structure and chemical composition. J. Aerosol Sci. 41 (1), 108–117.
Vander Wal, R.L., Bryg, V.M., Hays, M.D., 2011. XPS analysis of combustion aerosols for chemical composition, surface chemistry, and carbon chemical state. Anal. Chem. 83 (6), 1924–1930.
Vander Wal, R.L., Bryg, V.M., Huang, C.H., 2014. Aircraft engine particulate matter: Macro- micro- and nanostructure by HRTEM and chemistry by XPS. Combust. Flame 161 (2), 602–611.
Vander Wal, R.L., Bryg, V.M., Huang, C.H., 2016. Chemistry characterization of jet aircraft engine particulate matter by XPS: Results from APEX III. Atmos. Environ. 140, 623–629.
Vander Wal, R.L., Mueller, C.J., 2006. Initial investigation of effects of fuel oxygenation on nanostructure of soot from a direct-injection diesel engine. Energy Fuels 20 (6), 2364–2369.
Vander Wal, R.L., Tomasek, A.J., 2004. Soot nanostructure: dependence upon synthesis conditions. Combust. Flame 136 (1–2), 129–140.
Vander Wal, R.L., Tomasek, A.J., Street, K., Hull, D.R., Thompson, W.K., 2004. Carbon nanostructure examined by lattice fringe analysis of high-resolution transmission electron microscopy images. Appl. Spectrosc. 58 (2), 230–237.
Vander Wal, R.L., Yezerets, A., Currier, N.W., Kim, D.H., Wang, C.M., 2007. HRTEM Study of diesel soot collected from diesel particulate filters. Carbon 45 (1), 70–77.
Wang, L., Song, C., Song, J., Lv, G., Pang, H., Zhang, W., 2013. Aliphatic C–H and oxygenated surface functional groups of diesel in-cylinder soot: Characterizations and impact on soot oxidation behavior. Proc. Combust. Inst. 34 (2), 3099–3106.
Wei, J., Song, C., Lv, G., Song, J., Wang, L., Pang, H., 2015. A comparative study of the physical properties of in-cylinder soot generated from the combustion of n-heptane and toluene/n-heptane in a diesel engine. Proc. Combust. Inst. 35 (2), 1939–1946.
Yang, P.M., Wang, C.C., Lin, Y.C., Jhang, S.R., Lin, L.J., Lin, Y.C., 2017. Development of novel alternative biodiesel fuels for reducing PM emissions and PM-related genotoxicity. Environ. Res. 156, 512–518.
Yehliu, K., Armas, O., Vander Wal, R.L., Boehman, A.L., 2013. Impact of engine operating modes and combustion phasing on the reactivity of diesel soot. Combust. Flame 160 (3), 682–691.
Yehliu, K., Vander Wal, R.L., Armas, O., Boehman, A.L., 2012. Impact of fuel formulation on the nanostructure and reactivity of diesel soot. Combust. Flame 159 (12), 3597–3606.
Yoshida, A., Kaburagi, Y., Hishiyama, Y., 2006. Full width at half maximum intensity of the G band in the first order Raman spectrum of carbon material as a parameter for graphitization. Carbon 44 (11), 2333–2335.
Zaida, A., Bar-Ziv, E., Radovic, L.R., Lee, Y.J., 2007. Further development of Raman microprobe spectroscopy for characterization of char reactivity. Proc. Combust. Inst. 31 (2), 1881–1887.
Zardini, A.A., Suarez-Bertoa, R., Forni, F., Montigny, F., Otura-Garcia, M., Carriero, M., et al., 2019. Reducing the exhaust emissions of unregulated pollutants from small gasoline engines with alkylate fuel and low-ash lube oil. Environ. Res. 170, 203–214.
Zhu, J., Chen, Y., Shang, J., Zhu, T., 2019. Effects of air/fuel ratio and ozone aging on physicochemical properties and oxidative potential of soot particles. Chemosphere 220, 883–891.
Zolin, A., Jensen, A.D., Jensen, P.A., Dam-Johansen, K., 2002. Experimental study of char thermal deactivation. Fuel 81 (8), 1065–1075.